

Journal of
Applied Remote Sensing



Increased potential to monitor water quality in the near-shore environment with Landsat's next-generation satellite

Aaron D. Gerace
John R. Schott
Robert Nevins



SPIE

Increased potential to monitor water quality in the near-shore environment with Landsat's next-generation satellite

Aaron D. Gerace,^a John R. Schott,^a and Robert Nevins^b

^aRochester Institute of Technology, Center for Imaging Science, 54 Lomb Memorial Drive, Rochester, New York 14623
gerace@cis.rit.edu

^bSt. Olaf College, Department of Physics, 1500 St. Olaf Avenue, Northfield, Minnesota 55057

Abstract. The Operational Land Imager (OLI) is a new sensor developed by the joint USGS-NASA Landsat Data Continuity Mission that should become a valuable tool for studying inland and coastal waters. With upgrades to spectral coverage, 12-bit quantization, and increased signal-to-noise due to its new push-broom design, OLI exhibits the potential to become the first Landsat sensor with the radiometric resolution necessary for retrieval of the three primary constituents in Case 2 waters: chlorophyll, suspended materials, and colored-dissolved organic matter. Considering its traditional 30-m spatial resolution, this next-generation Landsat satellite will be especially useful for monitoring the near-shore environment. This work presents the relevant sensor parameters and results of experiments designed to determine if OLI will have the radiometric sensitivity necessary for water-based research. An OLI sensor model is developed, and its ability to retrieve water constituents from simulated data is compared with that of existing sensors. Results indicate that when atmospheric effects are properly accounted for, OLI introduces retrieval errors of less than 11% of the expected observable range for all three constituents. Furthermore, by spatially averaging a few OLI pixels, noise can be reduced to the Medium Resolution Imaging Spectrometer levels, making this next Landsat instrument an exciting option for monitoring inland and coastal waters. © The Authors. Published by SPIE under a Creative Commons Attribution 3.0 Unported License. Distribution or reproduction of this work in whole or in part requires full attribution of the original publication, including its DOI. [DOI: [10.1117/1.JRS.7.073558](https://doi.org/10.1117/1.JRS.7.073558)]

Keywords: Operational Land Imager; Landsat 8; Landsat Data Continuity Mission; water quality; parameter retrieval.

Paper 12428 received Nov. 9, 2012; revised manuscript received Feb. 20, 2013; accepted for publication Apr. 4, 2013; published online May 22, 2013.

1 Introduction

The ability to continuously monitor the global water supply from satellite imagery is an ongoing effort in the remote sensing community. Historically, water-based studies involving the use of satellite imagery have focused over the open ocean where the optical properties of these Case 1 waters are dominated by phytoplankton and its associated material.¹ With the progression of space-based technologies, monitoring efforts have shifted to studying optically complex Case 2 waters, which are typically found in coastal regions or inland lakes and ponds. Case 2 waters are classified as optically complex as they contain significant levels of inorganic suspended materials and colored-dissolved organic matter (CDOM), in addition to phytoplankton.

Although several instruments have the ability to monitor offshore Case 2 waters, no single existing satellite exhibits the necessary qualities for simultaneously monitoring the three primary coloring agents in the spatially complex near-shore environment. The ideal satellite would have the characteristics illustrated in Table 1; high spatial resolution to resolve the near-shore, high temporal resolution to capture the dynamic nature of water, high radiometric resolution to resolve the details in low signal levels, and data that is free to the community to foster research. Many satellites in orbit today exhibit several but not all of these characteristics.

The moderate resolution imaging spectroradiometer (MODIS) was designed with an appropriate spectral coverage and radiometric resolution necessary for studying water from space and

Table 1 Required characteristics for a satellite to be used to independently monitor the near-shore environment.

	MODIS	MERIS	Landsat 7	OLI	Commercial Products
Spatial Resolution	✗	✗	✓	✓	✓
Radiometric Resolution	✓	✓	✗	✓	✓
Temporal Resolution	✓	✓	✗	✗	✗
Free Data	✓	✓	✓	✓	✗

can be used to effectively monitor Case 1 and offshore Case 2 waters.² With a one-day repeat cycle, MODIS is particularly attractive for capturing the dynamic nature of water. Due to its 500-m spatial resolution over the visible and near-infrared (VNIR) spectrum, MODIS is not adequate for independently monitoring the spatially complex near-shore environment of coastal and inland waters. Figure 1 shows a true color image of western New York in the USA. The zoom windows to the right contain image data of the Rochester embayment collected by the MODIS and Enhanced Thematic Mapper Plus (ETM+) (Landsat 7) sensors on April 25, 2003, and the Medium Resolution Imaging Spectrometer (MERIS) data collected on May 9, 2011 (note: full resolution MERIS data was not openly available for April 25, 2003). Notice in the top right zoom window that the MODIS instrument is not able to resolve the smaller ponds with its 500-m resolution and that much of the detail in the river plume is lost.

Although Envisat became inoperable in early 2012, its primary sensor MERIS was particularly attractive as it was designed specifically for water-based research.³ Similar to MODIS, MERIS exhibited the temporal resolution necessary for monitoring Case 2 waters. It contained 15 narrow bands over the VNIR spectrum, a 12-bit system, and used a push-broom-style architecture giving it a high radiometric resolution. With 300-m pixels, MERIS was better equipped than MODIS to resolve the near-shore environment but still lacked the ability to capture the detail of many smaller inland lakes and ponds. The middle zoom window of Fig. 1 shows MERIS data over the Rochester embayment and while it was able to resolve a handful of pixels over the small ponds in the area, it still lacked the spatial resolution to adequately characterize the near-shore environment.

Alternatively, the 30-m spatial resolution of Landsat 7's ETM+ sensor is adequate for resolving the spatial detail found in near-shore Case 2 waters.⁴ The bottom zoom window in Fig. 1 shows ETM+ data over the Rochester embayment. Clearly it is superior to the other sensors in spatially resolving the near-shore environment (there are 100 Landsat 7 pixels to every 1 MERIS pixel). Yet, due to its radiometric characteristics, only limited success in retrieving levels of suspended sediment with this instrument has been demonstrated.^{5,6} With only four bands in the VNIR, an 8-bit quantizer, and limited signal-to-noise due to its whiskbroom design, Landsat's thematic mapper sensors lack the radiometric resolution necessary for simultaneously retrieving all three water quality parameters, where a significant change in constituents often leads to only a small change in sensor-reaching radiance. Additionally, with a 16-day repeat cycle, Landsat 7 lacks the ability to capture the time dynamic nature of water.

Many commercial airborne (and some space-based) instruments contain the necessary spatial, spectral, and temporal resolution required for monitoring water but have a significant charge associated with their data products precluding the repeat global coverage needed for scientific research. Therefore, no operational environmental sensor to date is ideal for independently monitoring Case 2 waters, indicating that monitoring efforts would benefit significantly by merging data from existing satellites.

A new sensor called the Operational Land Imager (OLI) has been developed by the joint USGS-NASA Landsat Data Continuity Mission (LDCM) and exhibits the potential to be both radiometrically and spatially suitable for monitoring Case 2 waters.⁷ While Landsat 5 and Landsat 7 have performed well beyond their five-year missions, efforts to extend the

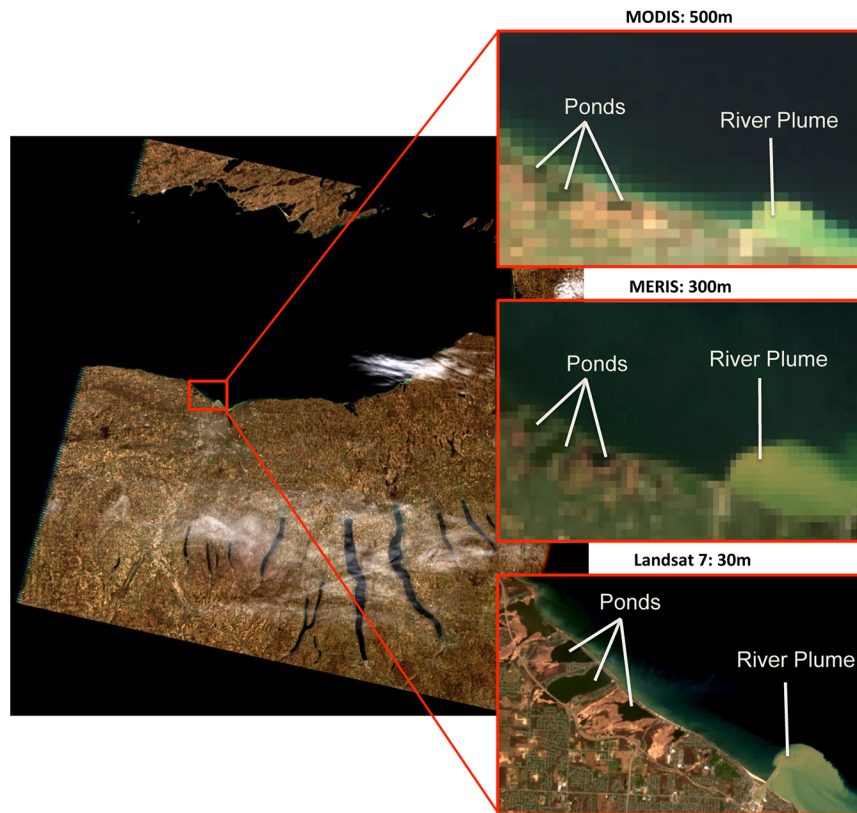


Fig. 1 True color image of the Rochester embayment located in western New York. From top to bottom, the zoom windows show image data gathered by the moderate resolution imaging spectroradiometer (MODIS), medium resolution imaging spectrometer (MERIS), and enhanced thematic mapper plus (ETM+) sensors, respectively. MODIS and ETM+ data was collected on April 25, 2003. MERIS data was collected on May 9, 2011.

collection of Landsat data became necessary in recent years. As a result of the LDCM's efforts, the OLI and the dual-band thermal infrared sensor were successfully launched on February 11, 2013, at 10:02 a.m. local time from Vandenberg Air Force Base. Equipped with eight 30-m VNIR/SWIR (shortwave infrared) bands and a 15-m panchromatic band, OLI has spectral and spatial coverage similar to that of ETM+. With features such as 12-bit quantization and improved signal-to-noise ratios (SNR) due to its push-broom-style architecture, the OLI instrument is radiometrically superior to its predecessor. When coupled with Landsat's native 30-m spatial resolution, OLI should provide the community with an additional water-monitoring sensor that fills in the near-shore data gap exhibited by all other environmental satellites. This is particularly exciting, as OLI will have the ability to monitor rivers and small ponds in addition to large lakes and seas.

This paper explores the potential for Landsat 8 to be used for monitoring water quality. Specifically, the new sensor characteristics of OLI are modeled and a retrieval methodology developed to determine if Landsat, a satellite program traditionally tailored for land-based research, will have the spectral coverage and radiometric resolution necessary for simultaneously retrieving the three primary water quality parameters found in Case 2 waters.

In the first study presented in this work, a model of OLI's relevant design parameters (enhanced spectral coverage, 12-bit quantization, and improved SNR due to its push-broom-style design) is developed based on the sensor's requirements,⁷ and its potential to retrieve chlorophyll, suspended materials, and CDOM concentrations from water is evaluated using simulated data. To gauge OLI's improved radiometric resolution over previous Landsat instruments and to determine its corresponding potential for water-constituent retrieval, the airborne visible/infrared imaging spectrometer (AVIRIS), MERIS, and ETM+ sensors are included in

this initial study. With 61 bands in the VNIR, 12-bit quantization, and high signal-to-noise, the AVIRIS hyperspectral sensor serves as a measure of the highest performance a sensor is likely to achieve in retrieving water constituents.⁸ Considering the AVIRIS sensor's inability to continuously monitor an area of interest due to its airborne platform, the MERIS instrument is included in this work to indicate the retrieval potential of an instrument designed specifically for water-based research. Finally, ETM+ is included to demonstrate the limitations of current Landsat instruments relative to the algorithms used here and to serve as a baseline to measure the improved features of OLI.

The second study presented in this work uses engineering test data of SNR to evaluate OLI's on-orbit constituent retrieval potential. SNR measurements from the OLI engineering test data are compared with actual in-orbit SNR measurements from advanced land imager (ALI) image data. The ALI is an instrument designed to test new Landsat technologies in space and is the pathfinder instrument for OLI. The constituent retrieval process is again performed using simulated data in this study, but with the improved SNRs observed in the engineering test data to determine OLI's retrieval potential assuming these noise levels can be maintained on orbit.

The results from the first two studies indicate that system noise is the main contributor to constituent retrieval error using the algorithms presented here. A final study is conducted that seeks to drive down system noise to further enhance constituent retrieval accuracy. In this study, the impact of averaging Landsat pixels on the retrieval process is investigated for a range of scenarios. The results of this study indicate that averaging just a few OLI pixels can drive down noise to levels that enable retrieval accuracy that is inline with MERIS.

Multiple sources can introduce error when using satellite imagery to retrieve constituents from water: inadequate knowledge of the inherent optical properties (IOPs) of the water; inability to properly characterize and remove atmospheric effects; using an uncalibrated sensor; and using a radiometrically deficient sensor. The experiments presented in this paper are sensor-only studies that seek to isolate the errors introduced to the constituent retrieval process by the aforementioned sensors when nadir-imaging. As these studies were specifically designed to gauge the radiometric potential of the OLI instrument; they are performed with the assumption that all sensors are radiometrically calibrated and that the atmosphere can be properly compensated for. In practice, the common empirical line method (ELM) for atmospheric correction satisfies both of these assumptions.⁹ As these studies seek to compare the relative performance of the OLI instrument to existing sensors, variability due to water IOPs is not treated in this work. By making the above assumptions, errors introduced to the retrieval process by the spectral and radiometric properties of the sensors are isolated.

2 Methodology

The goal of this work was to determine if the OLI sensor would be a useful tool for monitoring water quality, which would enhance the current suite of water-monitoring sensors, especially for observing the near-shore environment. Although Landsat 8 was launched in February 2013, its data are not yet available. However, a forward modeling approach can be used to simulate OLI data to determine its constituent retrieval potential. Referring to Fig. 2, an overview of the modeling process used in this research is described.

First, the in-water radiative transfer code Hydrolight¹⁰ is used to generate water-leaving radiance signals for a range of Case 2 waters when nadir-imaging. Next, as this study assumes knowledge of the atmosphere, these signals are passed through a known moderate resolution atmospheric transmission (MODTRAN) modeled atmosphere to generate top-of-the-atmosphere radiance spectra. The sensor models are used in the third stage of the modeling process to create simulated image data.

With simulated data in place, the constituent retrieval process can be initiated for each of the datasets by performing atmospheric compensation of the known atmosphere to obtain the retrieved water-leaving radiances associated with each imaged pixel. Last, a constituent retrieval algorithm (CRA) can be applied to invert these retrieved radiances to constituent concentrations. To describe the error introduced to the constituent retrieval process by each sensor, the average difference between the retrieved and actual constituent concentrations will be used as an error metric.

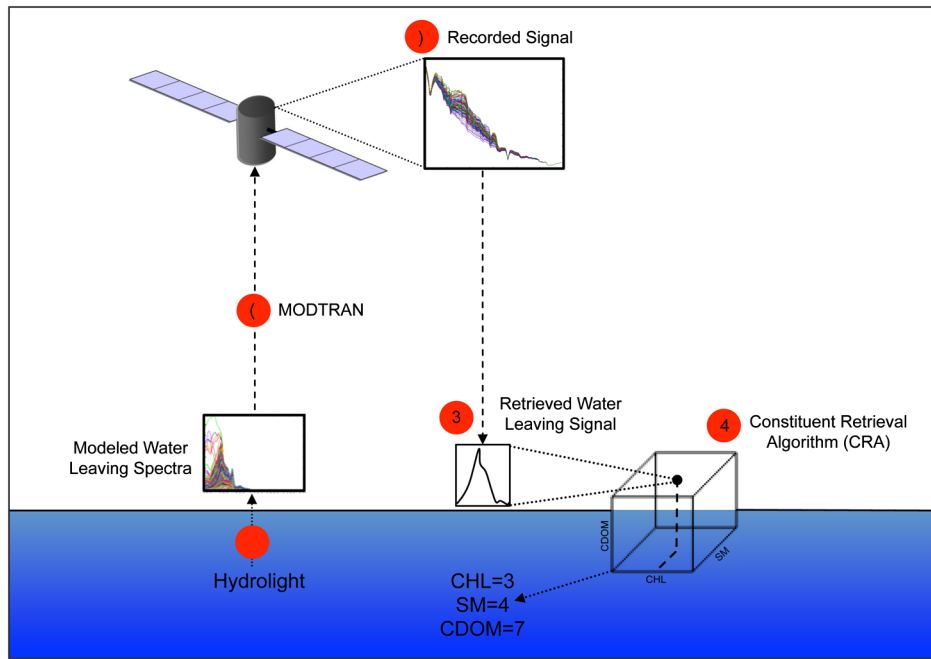


Fig. 2 Illustration of the modeling process used in this work.

2.1 Scene Simulation

With an overview of the methodology in place, the modeling process can now be discussed in more detail using Fig. 2 as a guide. The scene of interest for this study (shown in Fig. 1) is the Rochester Embayment of Lake Ontario and several coastal ponds and bays. This scene is favorable to evaluate the potential of the OLI instrument to perform constituent retrieval due to the wide range of water types in the area. The data used to drive this study were collected on May 20, 1999, by the Digital Imaging and Remote Sensing (DIRS) group at the Rochester Institute of Technology as part of a major ground truth campaign of the area where multiple radiometric measurements and water samples were obtained from the various lakes and ponds across the scene. These data were collected in conjunction with an AVIRIS over-flight. Therefore, an extensive knowledge of the region was developed, making it suitable for evaluating the potential of the OLI instrument.

2.1.1 In the water

Hydrolight is an in-water radiative transfer code that requires several environmental inputs from a scene of interest to determine the radiance leaving a water column.¹⁰ Figure 3 illustrates the various environmental inputs required by Hydrolight. To simulate the Rochester Embayment, Hydrolight requires solar zenith angle, wind speed, and the IOPs of the water as input. The four-component model is used to simulate data in this work so the spectral absorption/scattering coefficients and phase functions for chlorophyll, inorganic suspended materials, and pure water must be provided to Hydrolight (CDOM is treated strictly as an absorber, so only its spectral absorption coefficients are required). Due to the ground truth campaign conducted by the DIRS group, these inputs were well known for the scene of interest. Additionally, *in situ* water samples were obtained the day of the collect and processed in a lab to provide a range of observed constituent concentrations for the embayment. Therefore, to simulate a scene, Hydrolight was used to randomly create water samples that were representative of the wide range of water types shown in Fig. 1.

A random number generator was used in this work to create random water samples. By generating a uniformly distributed random number between 0 and 68 units for chlorophyll, a second uniformly distributed random number between 0 and 24 units for suspended materials, and a third uniformly distributed random number between 0 and 14 units for CDOM, a random water

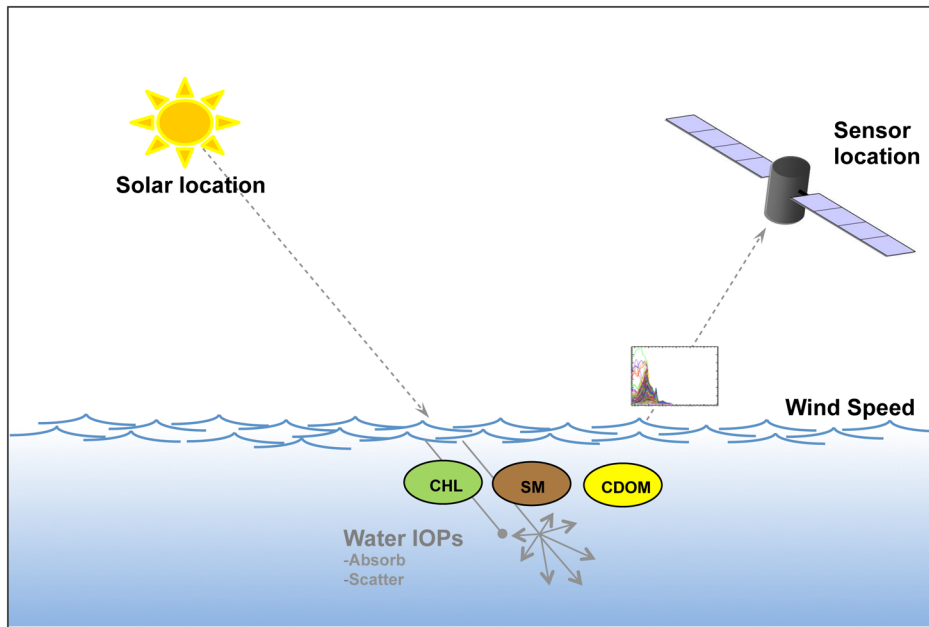


Fig. 3 Inputs required by the in-water radiative transfer code, Hydrolight.

type could be simulated in Hydrolight, i.e., these three numbers represent the concentrations of chlorophyll ($\mu\text{g/L}$), suspended materials (mg/L), and CDOM (1/m) that were used as input to Hydrolight, respectively. Hydrolight then outputs the water-leaving signal (expressed as spectral radiance just above the water surface) associated with the random water sample, which represents one pixel in the scene. This process was repeated thousands of times to simulate a scene. In this study, 2000 randomly generated pixels were created, as shown in Step 1 of Fig. 2. It should be noted that this is a particularly stressing approach, as it generates simulated water samples spanning the entire test space (e.g., low CDOM and high suspended materials, high CDOM and low suspended materials, etc.), even though this full range is unlikely in nature.

2.1.2 Through the atmosphere

MODTRAN code is an atmospheric radiative transfer model used in this work to simulate atmospheric effects.¹¹ Although perfect knowledge of the atmosphere is assumed in this study, the radiance signals estimated by Hydrolight must be propagated through an atmosphere to generate reasonable sensor-reaching radiance values before applying the modeled sensor characteristics, i.e., the Hydrolight output radiances are too dark for the SNR values used in this work, as they don't include upwelled radiance.

Considering the goal of this initial study was to provide the relative contribution of constituent retrieval error introduced by the four sensors, a rigorous attempt to accurately model atmospheric effects for any given date was not conducted. However, inputs to MODTRAN were provided to simulate atmospheric conditions that were representative of the scene shown in Fig. 1: a mid-latitude summer profile, urban aerosols, 35-km visibility, 16:00 GMT, lat = 43 N, lon = 77 W, 75-m elevation, 3% surface albedo for the surround, full VNIR spectrum. Figure 4 compares the total sensor-reaching radiance obtained from the MODTRAN simulation (green triangles) versus the at-sensor radiance for the R/G/B/NIR bands of Landsat 7 (red squares) and MODIS (blue diamonds) obtained over water from the April 25, 2003, data in Fig. 1. These data show that the simulations are within a few percent of the observations and differ from the observations less than the observations differ from each other.

The transmission and upwelled components of the MODTRAN output were used to generate sensor-reaching radiance according to

$$L_{s\lambda} = L_{w\lambda} * \tau_\lambda + L_{u\lambda}, \quad (1)$$

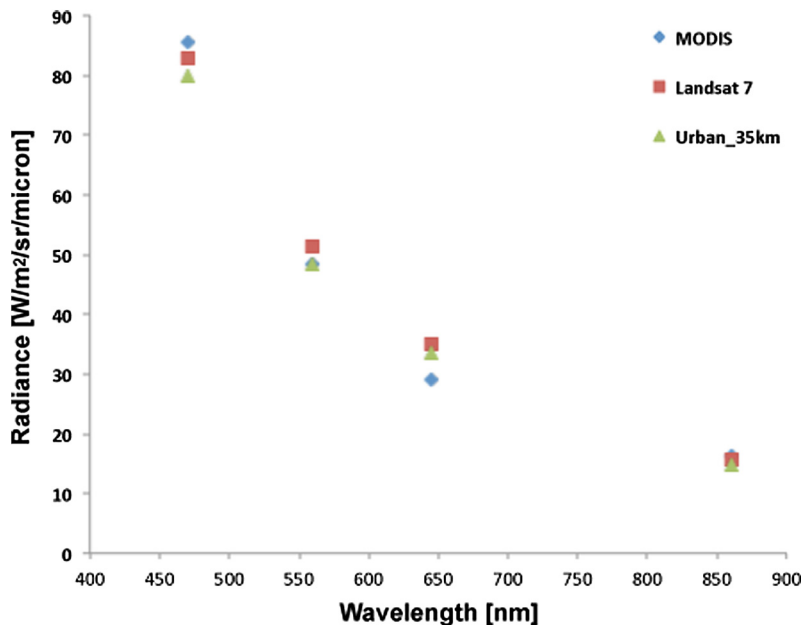


Fig. 4 Comparison of the total sensor-reaching radiance obtained from the moderate resolution atmospheric transmission (MODTRAN) simulation (green triangles) versus the at-sensor radiance for the R/G/B/NIR bands of Landsat 7 (red squares) and MODIS (blue diamonds) obtained over water from the April 25, 2003, data.

where $L_{s\lambda}$ represents spectral sensor-reaching radiance, $L_{w\lambda}$ represents the spectral water-leaving radiance signals simulated with HydroLight, and τ_λ , $L_{u\lambda}$ represent the spectral transmission and upwelled components simulated with MODTRAN, respectively.

Upon sampling the simulated sensor-reaching radiances by each sensor model to generate image data, atmospheric effects were removed from the image data according to

$$L_w = (L_s - L_u)/\tau. \quad (2)$$

Notice that the spectral component is removed from Eq. (2) as each term of Eq. (1) has been spectrally sampled by the sensor models to create image data. Accordingly, the transmission and upwelled components in Eq. (1) must be spectrally sampled to the sensor models to remove the known atmospheric effects.

Interestingly, although this work assumes perfect knowledge of atmospheric conditions, spectrally sampling the atmospheric components will introduce different levels of retrieval error as narrow-band sensors sample the atmosphere's spectral features better than broadband sensors. Therefore, although knowledge of atmospheric effects are assumed, some of the errors introduced by atmospheric effects are embedded in this modeling process.

2.1.3 At the sensor

The spectral sensor-reaching radiance signals indicated in Eq. (1) must be sampled by the key characteristics of the sensor models to simulate image data, see Fig. 5. First, the radiance signals are spectrally sampled to the response functions of each sensor. Next, random noise is applied to the signals based on SNR estimates. Last, the quantization process is simulated based on the dynamic range of each sensor. The end result of the sensor's sampling process is a discrete representation of the spectral sensor-reaching radiance signals. The implementation of each process is described in detail in the following sections.

Spectral sampling. The sensor-reaching radiance signals indicated in Eq. (1) were spectrally sampled to the sensor response functions of each sensor according to

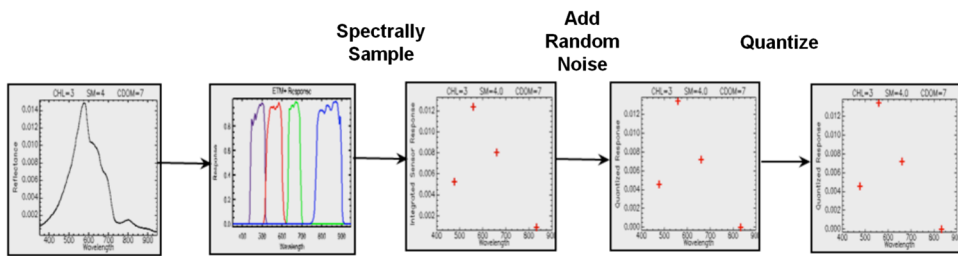


Fig. 5 Illustration of the key characteristics of the sensor models used in this study.

$$\int L_{s\lambda} * R_{\lambda i} * d\lambda_i / \int R_{\lambda i} * d\lambda_i \quad \text{for all bands,} \quad (3)$$

where $L_{s\lambda}$ is the spectral sensor-reaching radiance, $R_{\lambda i}$ is the spectral response function for band i , and $d\lambda_i$ is the corresponding wavelength spacing in band i .⁹ Since the absorption coefficients of pure water are several orders of magnitude higher in the SWIR than in the VNIR, the sensor-reaching signals are only spectrally sampled to each sensor's VNIR bands in this study.¹² Accordingly, in the VNIR, ETM+ has four bands,⁴ OLI has five bands,⁷ MERIS has 15 bands,³ and AVIRIS has 61 bands to spectrally sample the sensor-reaching signals.⁸

Noise implementation. In the next stage of the modeled sampling process, the signal is further altered by the introduction of sensor noise. In an effort to achieve higher SNRs, the OLI instrument is equipped with a push-broom-style architecture⁷ as opposed to the whiskbroom design of ETM+.⁴ Both types of instruments use linear array detectors to collect data, but a whiskbroom sweeps the data in the across-track direction as the satellite passes overhead in the along-track direction. Alternatively, push-broom sensors collect data in the along-track direction only, which is an advantage over the whiskbroom sensor as it can collect the same swath of data without any across-track movement. By eliminating this sweeping motion, a push-broom sensor avoids the need to scan allowing longer integration times resulting in increased signal-to-noise.

To simulate noise in this study, SNR system requirements⁷ were used for the OLI sensor model. To estimate SNR for the remaining sensors, actual radiance image data was obtained, and a region of interest containing several hundred pixels over water was defined. The mean signal level was divided by the standard deviation of the signals to calculate per-band SNR (see Fig. 6).

The resulting SNR values from Fig. 6 were used to estimate noise for the spectrally sampled signals according to

$$\text{SNR} = S/N \Rightarrow N_{L_i} = S_{L_i} / \text{SNR}_{L_i}, \quad (4)$$

where N_{L_i} is the noise associated with the spectrally sampled radiance signal (S_{L_i}) in band i , and SNR_{L_i} represents the calculated SNR (estimated SNR for OLI). Then, to add random noise for each band i of a signal, a random normal number $R(0, 1)$ was generated, multiplied by the noise estimate from Eq. (4) and the result added to the original signal according to

$$S_{L_i}(\text{w/noise}) = R(0, 1)N_{L_i} + S_{L_i}. \quad (5)$$

This process is repeated for all bands in each sensor and for all 2000 pixels in the simulated scene.

Quantizer implementation. Referring again to Fig. 5, the final process a signal encounters, as it is read by the sensor model, is the quantization process. OLI is equipped with a 12-bit quantizer,⁷ as opposed to the 8-bit dynamic range of ETM+.⁴ As a result, the continuous range of response values in a scene can be partitioned into 4096 (2^{12}), values for OLI while ETM+ allows for only 256 (2^8), such partitions. The result of this improved response resolution will be an increased radiometric resolution, as illustrated in Fig. 7, where the effective radiance range has been divided into 256 levels for ETM+ and 4096 levels for OLI.

The signal on the left hand side of Fig. 7 represents the spectral sensor-reaching radiance associated with an arbitrary water pixel. If this signal is spectrally sampled by the blue bands of

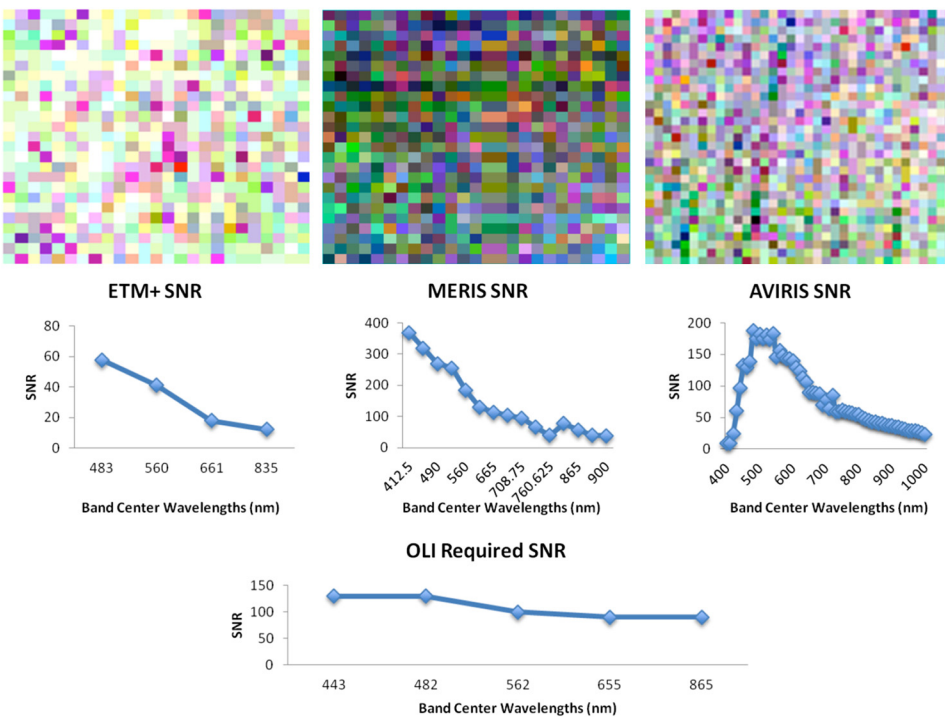


Fig. 6 Per-band signal-to-noise ratios (SNRs) used in the sensor models. SNR system requirements were used for Operational Land Imager (OLI) while SNR for the remaining sensors was calculated from radiance data over water.

ETM+ and OLI, bands 1 and 2, respectively, the blue (circle) values on the right-hand side of Fig. 7 are obtained. These values now need to be quantized (digitized) for the signal to be read out. To model the quantization process, the spectrally sampled radiance values (blue circle values) can be rounded to the nearest quantization level. The grey arrows on the right-hand side of Fig. 7 indicate that for every one quantization level that ETM+ has to place a spectrally sampled signal, OLI has 16 quantization levels. As a result, the 12-bit quantizer is better able to preserve the original signal.

The maximum radiance levels per band i ($L_{\max,i}$) that can be resolved by ETM+ and OLI are reported in Taylor (2011) and Irons and Masek (2006), respectively. From this, the step size (L_{Q_i}) of the quantization process can be approximated according to

$$L_{Q_i} (\text{step size}) = L_{\max,i} / 2^{(\text{of bits})}. \quad (6)$$

Once the step size (L_{Q_i}) is determined for each band i , the quantization levels can be set according to

$$L_{Q_{i,j}} = jL_{Q_i} \quad \text{for } j = 0, 1, \dots, n \quad \text{and} \quad 0 \leq L_{Q_{i,j}} \leq L_{\max,i}, \quad (7)$$

where $L_{Q_{i,j}}$ is the j 'th quantized radiance level in band i .

AVIRIS and MERIS both have 12-bit dynamic range, and the quantization process was modeled accordingly for their sensor models. The step sizes (L_{Q_i}) for these sensors were estimated from actual image data where calibration equations that relate digital number to sensor-reaching radiance were used in the estimation.^{3,8} The quantization levels were set according to Eq. (7), however, the maximum sensor-reaching radiance signal was used in place of $L_{\max,i}$ to gauge where to set the highest quantization level.

Finally, with the quantization levels set for each band in each sensor model, the 2000 signals were quantized by rounding their signal values in each band to the closest quantization level.

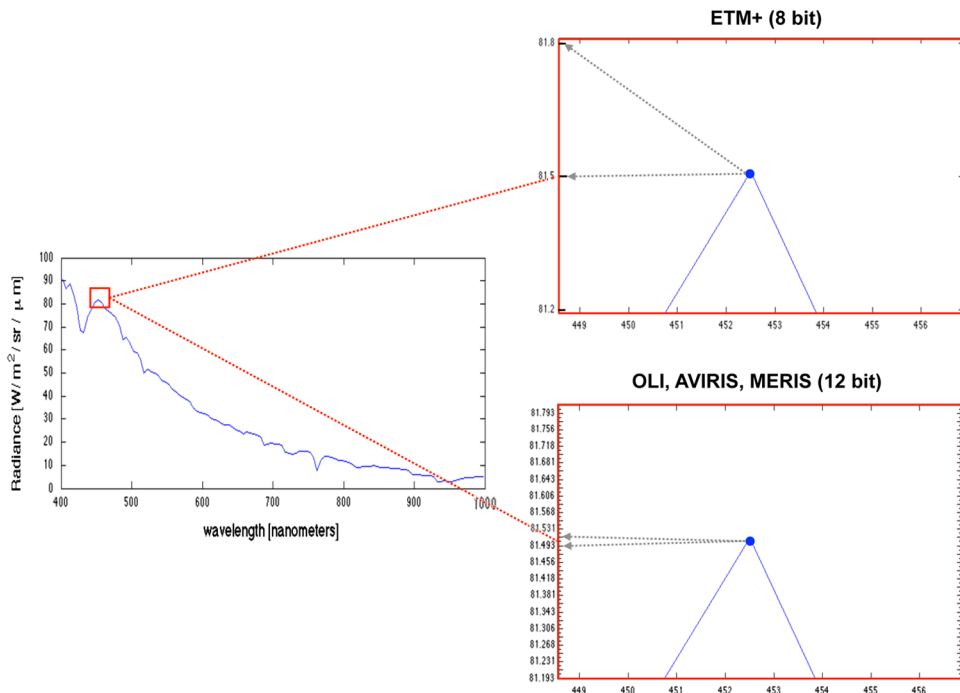


Fig. 7 Illustration of the response resolution associated with the 8-bit quantizer of ETM+ and the 12-bit quantizer of OLI, airborne visible/infrared imaging spectrometer (AVIRIS), and MERIS.

2.2 The Look-Up Table Constituent Retrieval Algorithm

The three aforementioned processes describe how a continuous sensor-reaching radiance signal is read in and digitized by a sensor model in this study. With a simulated scene in place (recall Step 3 from Fig. 2), the constituent retrieval process can be performed for each of the four sensors. In practice, to retrieve the water quality parameters using remotely sensed imagery, one would apply an atmospheric correction algorithm to retrieve the water-leaving radiances associated with the imaged water pixels. Then a CRA could be applied to invert the water-leaving radiances to constituent concentrations. Because we are only interested in the relative performance of sensors under test-case conditions in this study, an idealized atmospheric compensation was used for all sensors.

To initiate the constituent retrieval process in this experiment, the known (band-effective) atmospheric effects described in Sec. 2.1.2 are removed from the 2000 imaged water pixels according to Eq. (2) (Step 4 in Fig. 2). Next the CRA can be applied to determine the constituent concentrations associated with each imaged pixel (Step 5 in Fig. 2). While a variety of methods can be implemented to perform this task, a look-up table (LUT) inversion method was used in this study.¹³ LUTs are designed to provide the user with a library of “ground truth” spectra for a scene of interest. Figure 8 shows a sketch of the LUT used in this research. Notice that the axes

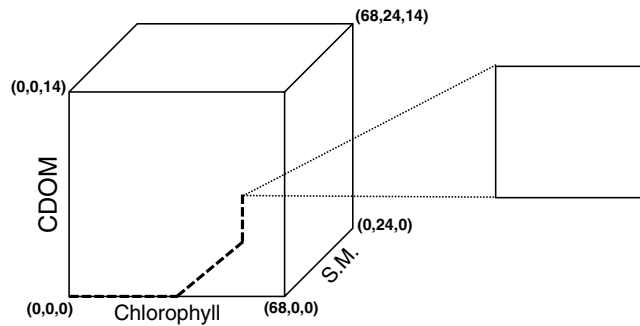


Fig. 8 Sketch of the look-up table (LUT) constituent retrieval algorithm (CRA) used in this study.

are defined by the various constituent concentrations in the scene and associated with each point in the three-dimensional space is a water-leaving radiance spectrum. If the LUT is populated sufficiently, it can be utilized by obtaining a water-leaving radiance spectrum from an image pixel, performing a search of the LUT for an adequate interpolated match, and observing the constituent concentrations associated with the match.

2.2.1 Look-up table development

A LUT should be populated with enough water samples to span the various water types across a scene. One way to populate such a LUT is through the process of collecting *in situ* observations. This procedure involves driving or rowing a boat out onto a water body, measuring the water-leaving signal with a spectrometer, taking a water sample, and determining its constituent concentrations through a filtering process performed in the lab. This must be done multiple times to obtain a LUT that is representative of all the water types in a scene. This is a daunting task for the multiple water types found in the Rochester Embayment shown in Fig. 1.

Alternatively, Hydrolight can be used to populate the LUT. In a process similar to the scene-generation process described in Sec. 2.1, the appropriate solar zenith angle, meteorological conditions, and IOPs can be provided as input to Hydrolight. Then, instead of supplying the model with random constituent concentrations as demonstrated in Sec. 2.1.1, input concentrations can be systematically varied to build a well-populated LUT. Table 2 shows the various constituent concentrations that were modeled in this work and the resulting water-leaving radiance spectra output.

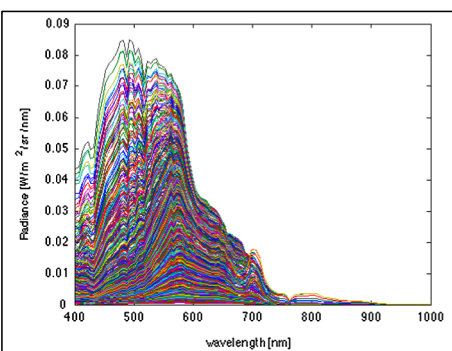
By supplying Hydrolight with every combination of constituent concentrations shown in Table 2, a well-structured and well-populated LUT was created. As shown in Fig. 8, the domain (axes) of the LUT define the levels of water constituents that are expected to be observed in the scene, while the range contains the associated water-leaving radiance spectra illustrated above. The end result of this process is a well-populated LUT that is ready to be used for the constituent retrieval process.

2.2.2 Constituent retrieval algorithm implementation

Recall that a retrieved water-leaving spectrum can be compared with the elements of the LUT in an effort to determine the constituents associated with the signal. Using a simple nearest neighbor to perform this comparison will introduce significant retrieval errors. Instead, the Levenberg-Marquardt nonlinear optimization algorithm was used to fit a least-squares cost function in this work.^{14,15} The implementation of the LUT CRA is illustrated in Fig. 9.

Table 2 Range of constituent levels used to develop the LUT CRA in this study and the corresponding simulated water-leaving radiance spectra.

CHL ($\mu\text{g/L}$)	SM (mg/L)	CDOM ($1/\text{m}$)
0	0	0
0.5	0.5	0.5
1	1	0.75
3	2	1
5	4	2
7	8	4
12	10	7
24	14	10
46	20	12
68	24	14



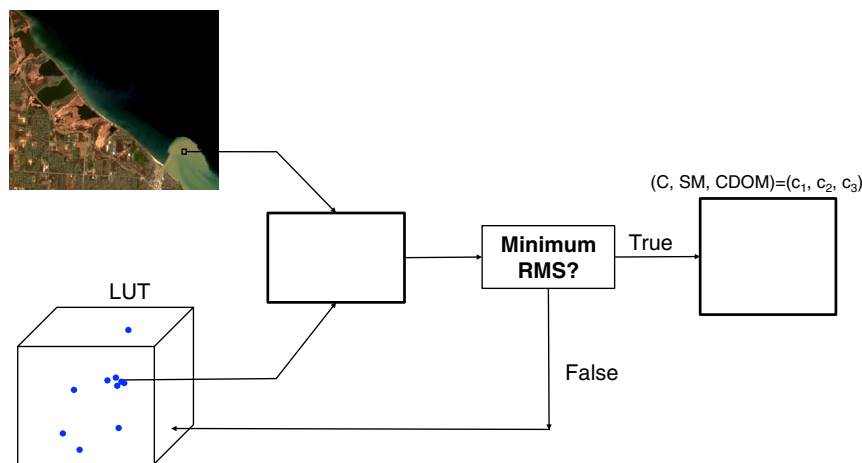


Fig. 9 Illustration of the search method used when implementing LUTs for the constituent retrieval process.

Using the spectrum associated with a pixel of interest (e.g., top-left of Fig. 9), the nonlinear optimization routine iterates through the LUT until the least-squares difference between the image-pixel spectrum and the interpolated LUT test spectrum falls below a predetermined threshold. The blue test points in the LUT of Fig. 9 illustrate how the optimization routine samples the test space until it converges on a solution. Once this occurs, the LUT coordinates associated with the matched spectrum represent the levels of chlorophyll, suspended materials, and CDOM associated with the image-pixel.

Errors will be associated with the retrieval process due to sensor degradation and the atmospheric removal process. Since this is a modeling effort, the concentrations of the constituents associated with each water-leaving signal are known as they were generated using Hydrolight (Step 1 of Fig. 2). The CRA estimates the constituent concentrations based on the retrieved water-leaving radiance signals (Step 5 of Fig. 2). The difference between the two can be used to define an error metric. In this work, the root mean square of the residuals between the retrieved and actual constituent concentrations for the 2000 water samples was expressed as a percentage of the observed range of constituents shown in Table 2. This provides a compact metric to compare the relative performance of the test sensors.

2.3 Retrieval Studies

To evaluate the new features of the OLI sensor and their corresponding error contributions to the constituent retrieval process, the initial study conducted in this work had three stages. In the first stage, the constituent retrieval process was performed in the absence of noise and quantization effects for the four sensors, i.e., the signals were only spectrally sampled before initiating the constituent retrieval process. A test of this nature determined how much constituent retrieval error could be attributed to just spectral coverage. Second, quantization was included into the sensor models to determine how dynamic range has an impact on a sensor's ability to retrieve water constituents. In the final stage, system noise was included into the sensor models. By spectrally sampling a signal, adding sensor noise, and quantizing the result, the effects of system noise on the sensor's abilities to retrieve water constituents could be gauged.

While the initial study described above used noise from OLI's initial requirements document, a second study was conducted in this work that used lab-measured noise margins from the actual OLI instrument as built. This second study provides a sense of the retrieval errors that may be achieved on orbit assuming the lab-measured noise measurements can be maintained on orbit.

OLI is an attractive sensor for monitoring the near-shore environment due to its 30-m resolution. However, radiometric resolution is imperative in these areas to achieve an accurate retrieval of in-water parameters. The final study presented here measures the impact of pixel averaging on radiometric resolution. The constituent retrieval process is performed after spatially

averaging OLI pixels for several scenarios and compared with the retrieval accuracy obtained by MERIS and AVIRIS.

3 Results

3.1 Initial Study

Figure 10 shows the errors associated with the retrieval of chlorophyll, suspended materials, and CDOM for each of the three stages. The errors are expressed as percent of the total range of constituents observed in the scene. Figure 10 (left) compares how well the four sensors retrieve water constituents when considering just their spectral coverage. All four sensors introduce constituent retrieval errors of less than 2% of the range shown in Table 2, indicating that spectral coverage is not the major contributor to retrieval error for this parameter set. This result is consistent with the findings of Sathyendranath et al.¹⁶ who determined that five bands of data can be as effective as spectral data in simultaneously distinguishing the levels of chlorophyll, suspended materials, and CDOM.

The second (middle) group in Fig. 10 compares the retrieval errors when spectral coverage and quantization effects are combined in the modeling process. Twelve-bits of quantization should better preserve a signal than 8-bits. This is clearly the case as the ETM+ sensor introduces significant errors in this stage, while the remaining 12-bit systems introduce retrieval errors of less than 3% for all constituents. This indicates that OLI's 12-bit quantizer is not a limiting factor in the constituent retrieval process.

Finally, the third (right) group of results illustrates how retrieval error is impacted when system noise is included in the analysis. Naturally, the radiometrically sensitive MERIS and AVIRIS systems introduce negligible error in this stage of the process. OLI introduces retrieval errors of less than 10% for two out of three constituents but is over 10% for chlorophyll retrieval. ETM+, on the other hand, introduces over 20% retrieval error for chlorophyll and CDOM and is over 10% for all three. This final stage indicates why, despite its attractive spatial resolution, it is difficult to use ETM+ for simultaneous constituent retrieval and why it has had limited success in monitoring Case 2 waters (this study indicates that ETM+ has significant value in mapping suspended materials as documented by Refs. 5 and 6). OLI, on the other hand, exhibits much greater potential to be used for simultaneous constituent retrieval.

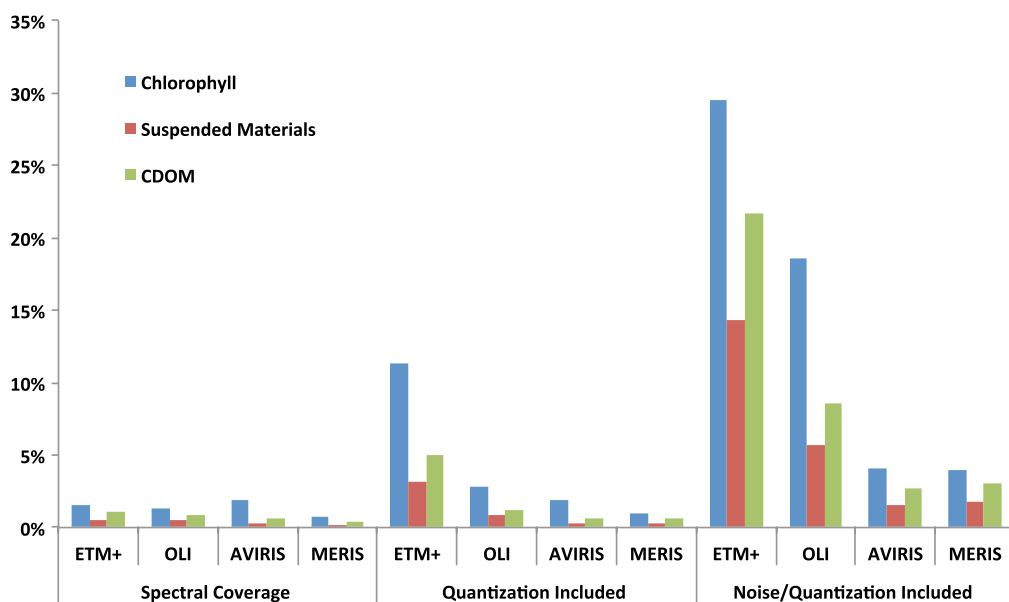


Fig. 10 Retrieval errors expressed as a percent of the range of concentrations observed in the scene.

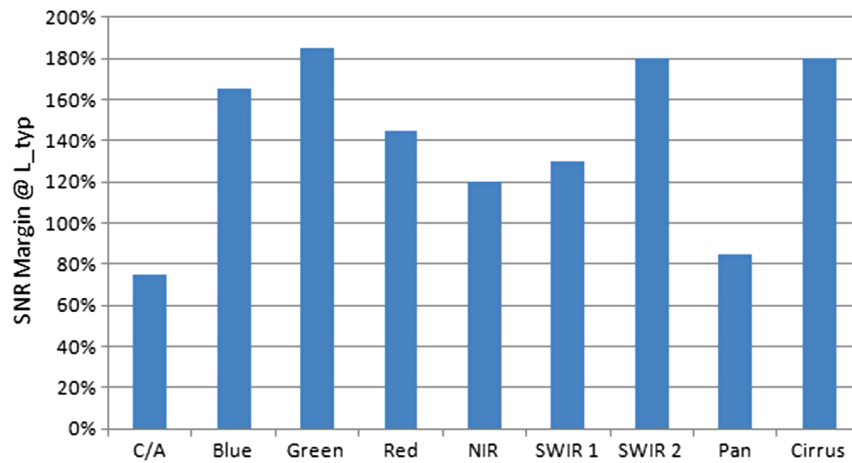


Fig. 11 SNR margins that may potentially be achieved with the final OLI instrumentation, i.e., percentage by which the SNR is expected to exceed the specified SNR value based on engineering test data.

3.2 Noise Margin Study

The SNR used in the previous study represent those published in OLI's requirements document⁷ and represent the minimum acceptable SNR. Engineering test data of the actual OLI instrument indicate that it should achieve significantly higher SNRs than the original required specifications. Figure 11 shows a bar chart of laboratory-measured SNR margins and represents the percentage above specification achieved in the lab. This chart indicates, for example, that laboratory-measured SNRs were 75% higher than specification for its coastal aerosol (C/A) band, 165% higher for its blue band, etc.

To gauge the credibility of the laboratory-measured noise margins shown in Fig. 11, SNR was calculated from an ALI image data over water according to Eq. (4). ALI is a system developed to validate in space new technologies for future Landsat missions.¹⁷ It contains the same spectral coverage and bit depth required by OLI and uses a push-broom-style architecture to collect its data. Figure 12 compares the SNR calculated from the ALI data to the lab-measured SNR values assuming that only half the margins of Fig. 11 could be achieved in orbit.

Interestingly, the half-margin SNR estimates from the OLI lab measurements are nearly identical to the SNR that is being achieved on-orbit with OLI's pathfinder instrument, ALI. Accordingly, two additional experiments were performed in this work to gauge OLI's retrieval potential under the assumption that it will achieve significantly higher SNR than originally

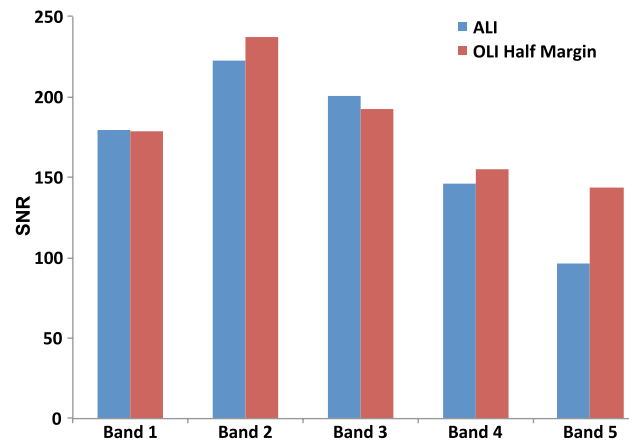


Fig. 12 Comparison of SNR values calculated from an advanced land imager (ALI) image over water to lab-measured SNR values assuming only half the margins shown in Fig. 11 can be achieved in orbit.

specified. First, the OLI sensor is modeled with SNRs that reflect half the margins shown in Fig. 11 and, second, the OLI sensor is modeled with SNRs that reflect the full margins shown in Fig. 11. The constituent retrieval process is performed with the same 2000 randomly generated pixels from the previous experiment to determine how these potentially improved SNRs will have an impact on OLI's retrieval ability. The results of this study are shown in Fig. 13.

Interestingly, if just half the margins described in Fig. 11 are achieved, OLI's potential ability to retrieve water constituents improves dramatically (Fig. 13: OLI Half Margin SNR). If the best-case scenario occurs and the OLI sensor achieves the full margins, expected retrieval errors will be under 10% for all three constituents, with the expected retrieval errors for suspended materials and CDOM under 5%.

3.3 Pixel Averaging Study

The results presented thus far have ignored the spatial resolution of the sensors and the impact of resolution on SNRs. Assuming all sensor parameters are equal, save detector size, a sensor that collects 300-m pixels will have higher SNR than a sensor that collects 30-m data as it receives 100 times the signal. Therefore, the results shown in Fig. 10 misrepresent the abilities of the ETM+, OLI, and AVIRIS sensors when compared with MERIS as they contain spatial resolutions of 30, 30, 20, and 300 m, respectively.

The next study presented in this work evaluates the potential to spatially average OLI pixels over water in an effort to enhance SNR and ultimately drive down retrieval errors. $A \cdot 2 \times 2$, $3 \times 3, \dots$, and 10×10 spatial average of simulated water pixels was performed to measure the impact of pixel averaging on retrieval error. The retrieval process described in Sec. 2 was applied using the same 2000 pixels. However, to simulate the spatial averaging process, n^2 random realizations of sensor noise (using the half-margin noise shown in Fig. 11) were applied to each of the 2000 pixels and averaged prior to submission to the constituent retrieval process for $n = 2, 3, \dots, 10$. The resulting retrieval errors are shown in Fig. 14.

Figure 14 shows that spatial averaging just a few OLI pixels will drive down retrieval errors to MERIS levels for suspended materials and CDOM. This is an important result for those monitoring suspended materials and CDOM in the near-shore environment, as it indicates that MERIS sensitivity can be achieved with OLI with minimal loss to spatial resolution (60 to 90 m pixels after the spatial averaging). Figure 14 also illustrates that chlorophyll retrieval is impacted more by system noise and requires more spatial averaging to drive down retrieval errors.

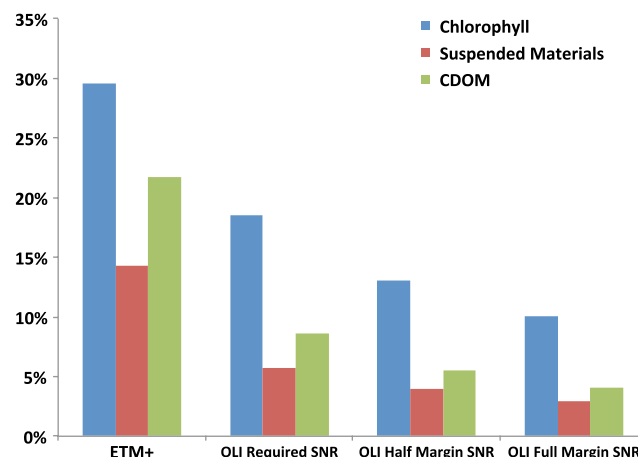


Fig. 13 Comparison of retrieval errors that can be achieved from the constituent retrieval process in the event that SNRs at half margin and SNRs at full margin can be achieved. These results are compared with retrieval errors obtained from simulated ETM+ data and simulated OLI data, which uses minimum required SNR values.

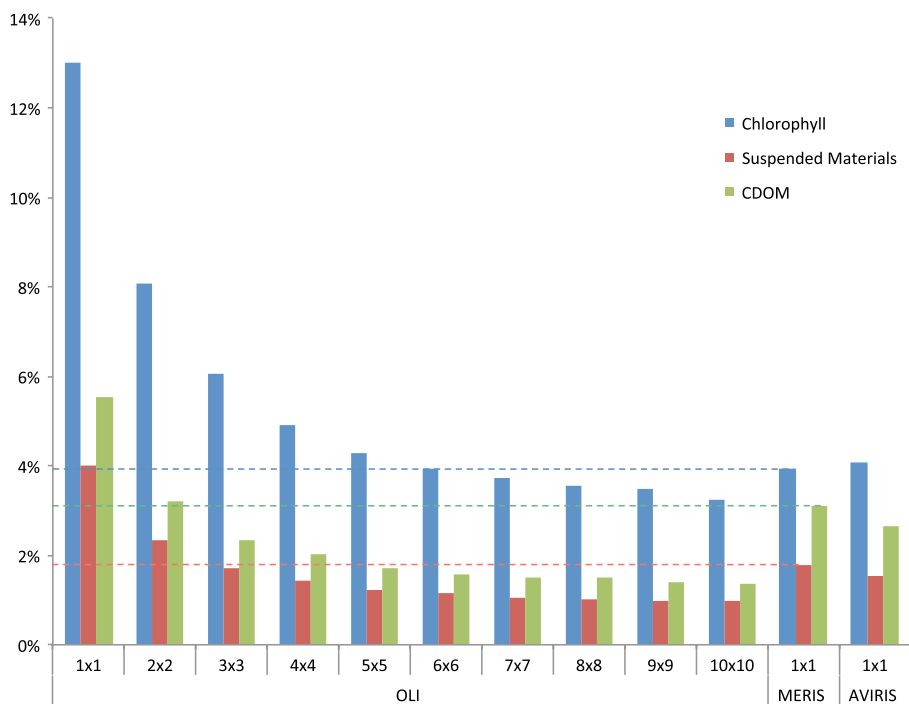


Fig. 14 Results of the constituent retrieval process when an $n \times n$ spatial average of OLI pixels is performed for $n = 1, 2, \dots, 10$. Half margin noise shown in Fig. 11 is used for this study.

An interesting observation can be made when “retrieved” concentrations are plotted versus “actual” concentrations for the three constituents studied here. Figure 15 shows plots of the concentrations obtained from the constituent retrieval process versus the actual concentrations used as input to the model for the 3×3 pixel averaging study described above. The plots for suspended materials and CDOM show that the retrieval errors are evenly distributed along the range of concentrations, save a minor loss of retrieval accuracy at lower concentrations for suspended materials and at higher concentrations for CDOM. Chlorophyll retrieval accuracy, on the other hand, exhibits a significant bias in retrieval errors towards higher concentrations.

To illustrate the importance of SNR when retrieving chlorophyll levels, Fig. 16 shows two Hydrolight-simulated water-leaving radiance spectra. Both water types were modeled using identical levels of suspended materials and CDOM but with high levels of chlorophyll that varied significantly (one contained $46 \mu\text{g/L}$ while the other contained $68 \mu\text{g/L}$). Note that the water-leaving spectra are nearly identical, but the difference in input concentrations is 32%. Figure 16 illustrates the importance of SNR and indicates that signal degradation due to system noise will adversely have an impact on chlorophyll retrieval at high levels where a significant change in concentration leads to only a small change in signal.

To further illustrate the impact of system noise on chlorophyll retrieval, Fig. 17 shows plots of the concentrations obtained from the constituent retrieval process versus the actual concentrations that were used as input to the model for the 3×3 , 6×6 , and 9×9 studies described

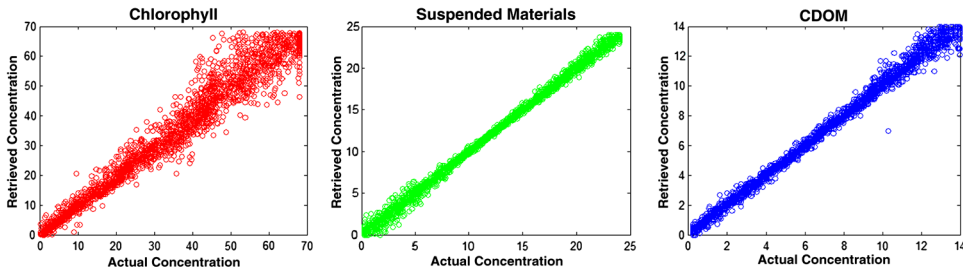


Fig. 15 Plots of retrieved concentrations versus actual concentrations from the 3×3 pixel averaging study for chlorophyll, suspended materials, and colored-dissolved organic matter (CDOM).

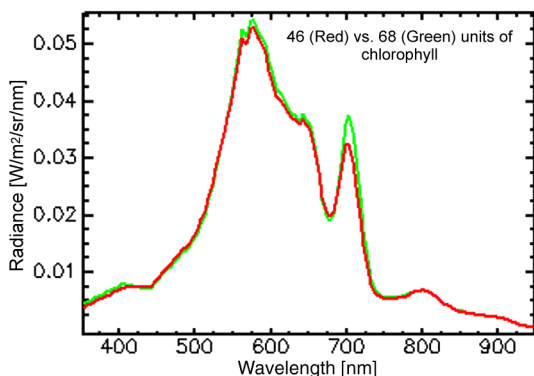


Fig. 16 HydroLight-modeled water-leaving radiance spectra for two water types. Suspended material and CDOM input concentrations were identical. The red curve used 46 units of chlorophyll as input while the green curve used 68 units of chlorophyll as input.

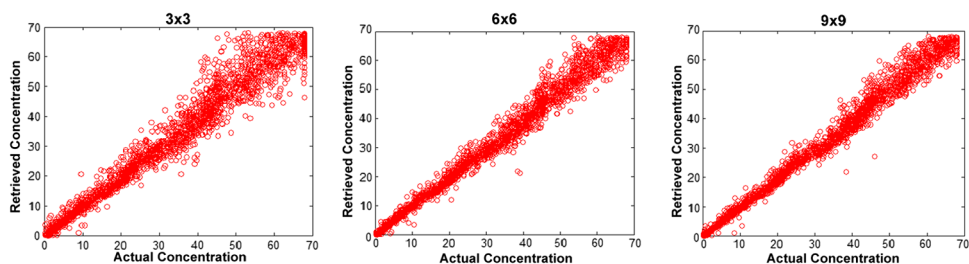


Fig. 17 Plots of retrieved concentrations versus actual concentrations from the 3×3 , 6×6 , and 9×9 pixel averaging study for chlorophyll.

above (the results of which are shown in Fig. 14). Notice that, as system noise is reduced by increasing the number of pixels averaged, the error in chlorophyll retrieval is reduced, especially at high concentrations.

4 Concluding Remarks

The OLI is a new Landsat sensor developed by the LDCM that exhibits the potential to be an invaluable tool for studying inland and coastal waters in the near-shore environment. With upgrades to spectral coverage, 12-bit quantization, and improved signal-to-noise, OLI is positioned to become the first Landsat instrument with the spectral coverage and radiometric resolution necessary for water-based research.

As with any in-water parameter-retrieval study, adequately removing atmospheric effects from the at-sensor OLI radiance data will be required to properly retrieve water constituent concentrations. When ground truth is available, the ELM is the preferred method for removing atmospheric effects as it introduces negligible error to the retrieval process. Since ground truth campaigns are not always a viable option, ongoing work focuses on the removal of atmospheric effects from OLI data in the absence of ground truth measurements. OLI will not be equipped with the two NIR bands required by traditional over-water atmospheric correction techniques for multispectral instruments,^{18,19} so alternative methods will be required. Gerace and Schott²⁰ identify an atmospheric correction technique that uses the ratio of OLI's NIR band 5 and SWIR band 6 instead of two NIR bands and demonstrates through a simulated case-study its potential to be used to adequately compensate for atmospheric effects.

The work described in this article demonstrates through a simulated case study that if atmospheric effects can be properly removed, OLI exhibits the radiometric sensitivity required for the simultaneous retrieval of chlorophyll, suspended materials, and CDOM in Case 2 waters. This is particularly exciting, as OLI will not only provide the water-monitoring community with an additional data source but, due to its 30-m spatial resolution, should help to fill in the near-shore data gap exhibited by all other operational environmental satellites.

References

1. A. Morel and L. Prieur, "Analysis of variations in ocean color," *Limnol. Oceanogr.* **22**(4), 709–722 (1977), <http://dx.doi.org/10.4319/lo.1977.22.4.0709>.
2. V. V. Salomonson et al., "MODIS: advanced facility instrument for studies of the earth as a system," *IEEE Trans. Geosci. Remote Sens.* **27**(2), 145–153 (1989), <http://dx.doi.org/10.1109/36.20292>.
3. European Space Agency (ESA), "MERIS Product Handbook," European Space Agency, Paris, France, ENVISAT Website, http://envisat.esa.int/pub/ESA_DOC/ENVISAT/MERIS/miris.ProductHandbook.2_1.pdf (24 October 2006).
4. M. P. Taylor, "Landsat 7: Science Data Users Handbook," NASA's Goddard Space Flight Center, Greenbelt, MD, NASA Website, http://landsathandbook.gsfc.nasa.gov/handbook/handbook_htmls/chapter8/chapter8 (11 March 2011).
5. K. P. Sudheer, I. Chaubey, and V. Garg, "Lake water quality assessment from Landsat thematic mapper data using neural network: an approach to optimal band combination selection," *IEEE Trans. Geosci. Remote Sens.* **27**(2), 145–153 (1989), <http://dx.doi.org/10.1109/36.20292>.
6. J. J. Wang et al., "Retrieval of suspended sediment concentrations in large turbid rivers using Landsat ETM plus: an example from the Yangtze River, China," *Earth Surf. Proc. Land.* **34**, 1082–1092 (2009), <http://dx.doi.org/10.1002/esp.v34:8>.
7. J. R. Irons and J. G. Masek, "Requirements for a Landsat data continuity mission," *Photogramm. Eng. Remote Sens.* **72**(10), 1102–1108 (2006).
8. G. Vane et al., "The airborne visible/infrared imaging spectrometer (AVIRIS)," *Remote Sens. Environ.* **44**, 127–143 (1993), [http://dx.doi.org/10.1016/0034-4257\(93\)90012-M](http://dx.doi.org/10.1016/0034-4257(93)90012-M).
9. J. R. Schott, *Remote Sensing: The Image Chain Approach*, 2nd ed., Oxford University Press, New York, NY (2007).
10. C. Mobley, *Light and Water*, Academic Press, Inc., San Diego, CA (1994).
11. A. Berk, L. S. Bernstein, and D.C. Robertson, "MODTRAN: a moderate resolution model for LOWTRAN 7," Air Force Geophysics Laboratory Technical Report GL-TR-89-0122, Hanscom AFB, MA (2000).
12. V. M. Zolotarev and A. V. Demin, "Optical constants of water over a broad range of wavelengths, 0.1 Å–1 m," *Opt. Spectrosc.* **43**(2), 157–161 (1977).
13. C. D. Mobley et al., "Interpretation of hyperspectral remote-sensing imagery via spectrum matching and look-up tables," *Appl. Opt.* **44**, 3576–3592 (2005), <http://dx.doi.org/10.1364/AO.44.003576>.
14. K. Levenberg, "A method for the solution of certain nonlinear problems in least squares," *Q. Appl. Math.* **2**, 164–168 (1944).
15. D. W. Marquardt, "An algorithm for least-squares estimation of nonlinear parameters," *J. Soc. Ind. Appl. Math.* **11**(2), 431–441 (1963), <http://dx.doi.org/10.1137/0111030>.
16. S. Sathyendranath, L. Prieur, and A. Morel, "A three-component model of ocean colour and its application to remote sensing of phytoplankton pigments in coastal waters," *Int. J. Remote Sens.* **10**(8), 1373–1394 (1989), <http://dx.doi.org/10.1080/01431168908903974>.
17. R. Bryant et al., "Data continuity of Earth observing 1 (EO-1) advanced land imager (ALI) and Landsat TM and ETM+," *Trans. Geosci. Remote Sens.* **41**(6), 1204–1214 (2003), <http://dx.doi.org/10.1109/TGRS.2003.813213>.
18. H. R. Gordon and M. Wang, "Retrieval of water-leaving radiance and aerosol optical thickness over the oceans with SeaWiFS, a preliminary algorithm," *Appl. Opt.* **33**(3), 443–452 (1994), <http://dx.doi.org/10.1364/AO.33.000443>.
19. K. G. Ruddick, F. Ovidio, and M. Rijkeboer, "Atmospheric correction of SeaWiFS imagery for turbid coastal and inland waters," *Appl. Opt.* **39**(6), 897–912 (2000), <http://dx.doi.org/10.1364/AO.39.000897>.
20. A. D. Gerace and J. R. Schott, "Over-water atmospheric correction for Landsat's new OLI sensor," *Proc. SPIE* **8372**, 837211 (2012), <http://dx.doi.org/10.1117/12.919304>.

Biographies and photographs of the authors are not available.